Review

Multi-gap Resistive Plate Chambers for Time of Flight applications

Yi Wang [1,*] and Yancheng Yu [1]

[1] Key Laboratory of Particle and Radiation Imaging, Department of Engineering Physics, Tsinghua University, Beijing 100084, China; yiwang@mail.tsinghua.edu.cn (Y.W.); yuyc2019@163.com (Y.Y.)

* Correspondence: yiwang@mail.tsinghua.edu.cn; Tel.: +86-13331129352

Abstract:

Multi-gap Resistive Plate Chamber has been attracting increasing attention and has been studied in recent decades because of its good efficiency, high time resolution and relatively low cost. It has become a new standard technology for the Time of Flight system in particle and high energy physics experiments. In this paper, we introduce the operation principle and structure of the MRPC detector and review the applications on the Time of Flight system in several famous experiments, such as STAR, CBM and SoLID. The performances including time resolution and particle identification are discussed in detail. Some recent advances and perspectives with regard to the future development of the next generation MRPC are also outlined.

Keywords: Multi-gap Resistive Plate Chamber; Time of Flight; particle identification; Time resolution; high energy physics experiments;

1. Introduction

Time of Flight (ToF) system is an essential part for particle identification (PID) [1] in particle and high energy physics experiments. In order to identify hadrons, their charge and mass need to be determined. Since the mass of the particle can't be obtained directly, it has to be calculated from the measurement of momentum and velocity. A magnetic spectrometer measures the momentum, while ToF detectors determine the velocity of the charged particle by measuring the time required to travel from the interaction point to the time of flight detector, or between two detectors. There are mainly three typical detectors that would be considered to construct the ToF system. (1) The parallel plate chambers (PPC) [2, 3] was thoroughly investigated at CERN in the early 1990s for possible use at the LHC. The PPC with two metallic electrodes is a single-gap gaseous detector operating in the avalanche mode. To avoid a transition to streamer, the gas gain should be kept low. Therefore, PPC with wide gas gap has bad time resolution due to the long duration of the avalanche buildup and the signal of narrow-gap PPC is quite weak. Those reasons lead to a difficulty with the high efficiency (greater than 90%) and good timing resolution (better than 250 ps). (2) Scintillators with photomultipliers are very commonly used due to their good time resolution. For example, the LIDAL system [4] use fast plastic scintillators read by Photo-Multiplier-Tubes (PMTs) to perform ToF measurements. Tests of proton beam have shown that time resolution bellow 100 ps have been achieved. However, since the particle experiments are usually large in size and the PMTs are expensive, the cost per area becomes an important issue. (3) (Multi-gap) Resistive plate chamber (RPC) is a relatively new and standard technology for ToF system. It is known for very high detection efficiency (>95%), excellent time resolution (<100 ps) and relatively low cost. This detector is easy to build and possible to cover a large area. It has been widely used in many physics experiments, such as ALICE [5, 6], BESIII [7], CBM [8, 9], STAR [10-12] and PHENIX [13].

This review will focus on multi-gap resistive plate chamber (MRPC) and its applications as a ToF detector in large experiments. The description and detector physics of MRPC are introduced

briefly in Sect 2. Its applications in current large experiments and developments for future TOF systems are discussed in Sect 3.

2. Description of MRPC Detector

In the 1980s, Santonico [14] built the first prototype of the RPC, which can be seen as the successor of the metallic Parallel Plate Chambers (PPC) with resistive electrodes. The use of resistive electrodes allow the detector self-quenching and restrict discharges to a local area, which makes RPCs easy to build and work stably. For trigger applications, typical RPCs can operate at around 95% efficiency with a time resolution much better than the nanosecond scale and at a counting rate of hundreds Hz/cm^2. However, if we want to improve the time resolution, the effective way is to relatively reduce the gap width and greatly increase the electric field. Since the avalanches would continue to grow until the occurrence of large streamers, the detector would not work well. To stop the avalanche growing and improve the performance of normal RPCs, the multi-gap RPC [15] is introduced in 1996.

As shown in Figure 1, the idea is to simply add more resistive plates in a wide gas gap so that the gap is now divided into many smaller gaps. Commonly nylon fishing lines are used to confirm a homogeneous gap width. Thus, the avalanche is limited into a small space and the electric field can be increased, which leads to a much better time resolution. The high voltage is just applied to the graphite layer coated on the outer resistive plates of each stack, while the intermediate resistive plates are allowed to electrically float. Moreover, to ensure insulation between the HV electrodes and the readout strips, a thin layer of Mylar is used and glued on the PCB (printed circuit board) copper layer. All the charge moving in any of the gas gaps will induce charge on the pickup electrodes. The signals with both polarities can read out at both ends using front end electronics. The honeycomb boards are attached on the top and bottom to support the whole detector.

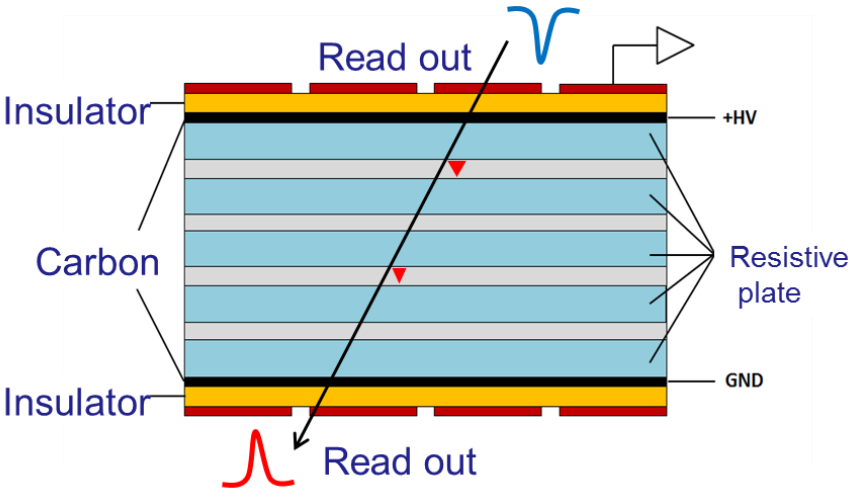

Figure 1. Schematic sketch of a multi-gap resistive plate chamber (MRPC).

Even though the geometry of the detector is simple as shown above, the physics in MRPCs is very complex. The detector physics analyses and detailed simulations are well studied and can be found in Ref. [16-20]. The main features in the operation of these detectors are the fact that the electric field is high and uniform and gas gap is subdivided into many small gaps. Therefore, a passing particle produces individual and separate clusters of primary ionization; each cluster will start an avalanche immediately and the final signal induced on the pickup electrodes will be the sum of all avalanches from all gaps. Fluctuations within the avalanche mechanism dominate the single-gap behavior while an average of many avalanches is the resultant signal in MRPCs. There are many other advantages of the MRPC technology. For example, the chamber operates at

atmospheric temperature and pressure; the resistive electrodes quench streamers so that they do not initiate a spark breakdown, which allows for high-gain operation; the construction technique is rather simple and generally based on commercially available and cheap materials; there is no late tail in the time response and the charge spectrum has a peak well separated from zero, thus the setting of the threshold is far less critical with respect to exponential-shaped charged spectra.

3. Applications in Large Experiments

Since the early 2000s, MRPCs have been carefully investigated and have become the new standard TOF technology as can be seen by many physics experiments. Several typical experiments and their MRPC-based TOF will be reviewed in this section.

3.1. STAR experiment in RHIC

The Brookhaven National Laboratory's Relativistic Heavy Ion Collider (RHIC) [21] is the first machine in the world capable of colliding heavy ions. The Solenoidal Tracker at RHIC, known as STAR [22], utilizes a large cylindrical Time-Projection Chamber (TPC), installed inside a large solenoid magnet, providing a close to 4π angle tracking capability for charged particles from collisions. It is used to search for signatures of the form of matter that RHIC was designed to create: the quark-gluon plasma (QGP). The full-acceptance MRPC-based TOF system [23] was proposed to match the acceptance of the TPC, the Silicon Vertex Tracker (SVT), and the Barrel Electromagnetic Calorimeter (BEMC). It can extend STAR's capability for kaon separation from ~0.6 to ~1.7 GeV/c; the range for proton separation would be increased from approximately ~1 GeV/c to ~3.0 GeV/c. This extension of the momentum range for particle identification is crucial to enable a number of key measurements that can't be achieved otherwise.

3.1.1. The STAR MRPC

The structure of MRPC module appropriate for STAR is shown in Figure 2. The upper view in this figure shows the long edge of a module, while the lower shows the short edge. This MRPC has 6 gaps of 0.22 mm thick in a single stack. It is assembled with float glass of typical resistivity on the order of 10^{12} Ω/cm. The outer and inner glass plates are 0.7 and 0.54 mm thick, respectively. It operates in avalanche mode with a non-flammable gas mixture of 95% F134a and 5% iso-butane. The electric field in the gas gap is around 106 kV/cm.

Each module consists of six read-out pads, each of 3.1×6.0 cm^2. There is a 3-mm gap between each pad. The differential signal is read out and amplified by NINO chip [24, 25] developed at CERN, which is an ultrafast front-end preamplifier-discriminator chip with a peaking time of 1 ns, low power consumption of 30 mW/channel and a resolution of 20 ps rms. The ASIC TDC used in STAR-TOF is the CERN HPTDC ASIC [26-28]. The HPTDC uses a tapped delay line architecture to perform its time-sampling function. The 40 MHz input clock is multiplied on the chip to 320 MHz with a phase locked loop (PLL). Its time resolution is around 25ps.

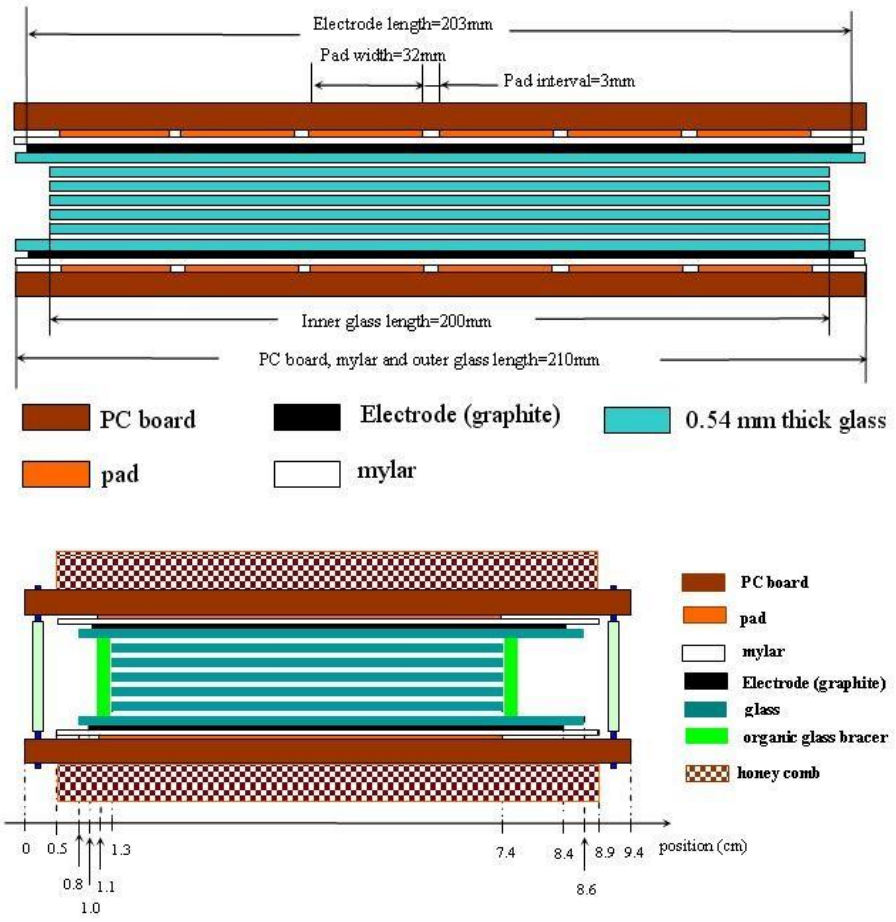

Figure 2. Two side views of the structure of an MRPC module. The upper (lower) view shows the long (short) edge.

3.1.2. The STAR-ToF system

The cylindrical TOF detector covers a total area of approximately 64 m^2. There will be 32 MRPC modules in each of 120 trays, and 3840 total modules. Tsinghua University and University of Science and Technology of China (USTC) are responsible for the MRPC production. To assure the quality of MRPC modules, a complete set of instructions and procedures for manufacturing techniques and quality assurance (QA) system [12] were setup in Tsinghua University. The picture of a batch of MRPC for STAR-TOF produced in Tsinghua University is shown in Figure 3. Beam tests [11] in the PS T10 beam line at CERN showed that the overall time resolution after time slewing correction can reach 60 ps and an efficiency of 97% were achieved.

The R&D and production of STAR-ToF was started in 2000 and completed in 2009. The final trays ran stably in different physics runs. The overall, start, and stop time resolutions of the ToF prototypes and final system trays are summarized in Table 1. The leading and trailing edges of a detector signal are digitized in the same channel of an HPTDC chip starting from Run5 and the slewing corrections were then based on the ToT values. For earlier runs, the slewing corrections were based on the signal area using CAMAC ADC values. The stop resolution of the final system trays (Run8 and later) is around 80 ps, which meets the physics requirement.

Figure 3. The picture of a batch of MRPC for STAR-TOF produced in Tsinghua University.

Table 1. The total time resolution from the STAR TOF system during different physics run.

Operation condition			Time resolution (ps)		
			Start time	Overall	Stop time
Run 3	200GeV d+Au		~85	~120	~85
	200GeV p+p		~140	~160	~80
Run 4	62GeV Au+Au		~55	~105	~89
	200GeV Au+Au	FF/RFF	~27	~74	~70
		HF	~20	~74	~71
Run 5	200GeV Cu+Cu (TOT)		~50	~92	~75
	64GeV Cu+Cu (TOT)		~82	~125	~94
Run 8 5 Trays	200GeV p+p (TOT)		~83	~112	~75
Run 9 86 Trays	500GeV p+p (TOT)		~85	~117	~78

3.1.3. The PID performance

In the 200 GeV d+Au collisions, the average MRPC TOF timing resolution alone was measured to be 85 ps. Hits from particles traversing the TPC were reconstructed as tracks with well-defined geometry, momentum, and dE/dx. The particle trajectory was then extended outward to the TOF detector plane. Figure 4(a) [30] shows inversed velocity (1/β) from TOFr measurement as a function of momentum (p) calculated from TPC tracking in TOFr triggered d+Au collisions. Separations between pions and kaons, kaons and protons are achieved up to $p_T \simeq 1.6$ and 3.0 GeV/c, respectively. The insert shows $m^2 = p^2(1/\beta^2 - 1)$ for $1.2 < p_T < 1.4$ GeV/c. Clear separation of pions, kaons and protons can be seen. In addition to its hadron identification capability, it allows electrons/positrons to be identified at low momentum ($p_T < 3$ GeV/c) by using a combination of velocity information (β) from TOFr and dE/dx measured in the TPC [31]. Figure 4(b) [32] demonstrates the clean separation of electrons from hadrons using their dE/dx in the TPC after applying a ToF cut of $|1/\beta - 1| \leq 0.03$. This cut eliminated the hadrons crossing the electron dE/dx band.

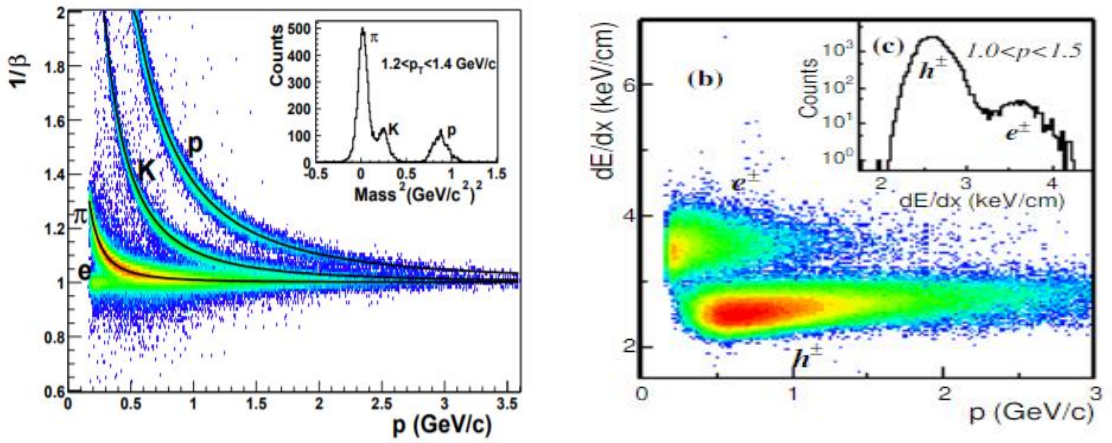

(a) **(b)**

Figure 4. (a) 1/β vs. momentum for $\pi^{\pm}$, $K^{\pm}$, and p ($\bar{p}$) from 200 GeV d+Au collisions. **(b)** dE/dx in the TPC vs. particle momentum (p) with a TOF cut of $|1/\beta - 1| \leq 0.03$. Insert: projection on the dE/dx axis for particle momenta 1< p <1.5 GeV/c.

Another example that shows the synergy between dE/dx and the TOF is illustrated with the observation of antimatter Helium-4 [33], as shown in Figure 5. The top two panels show the dE/dx in units of multiples of $\sigma_{\mathrm{dE/dx}}$, $n_{\sigma_{\mathrm{dE/dx}}}$, of negatively charged particles (first panel) and positively charged particles (second panel) as a function of mass measured by the TOF system. The masses of ^{3}He ($\overline{^3He}$) and ^{4}He ($\overline{^4He}$) are indicated by the vertical lines at 2.81 GeV/c² and 3.73 GeV/c², respectively. The horizontal line marks the position of zero deviation from the expected value of dE/dx ($n_{\sigma_{\mathrm{dE/dx}}}$= 0) for ^{4}He ($\overline{^4He}$). The rectangular boxes highlight areas for ^{4}He ($\overline{^4He}$) selections. The bottom panel shows a projection of entries in the upper two panels onto the mass axis for particles in the window of $-2 < \sigma_{\mathrm{dE/dx}} < 3$. The combined measurements of energy loss and the time of flight allow a clean identification to be made. There is clear separation between $\overline{^3He}$ and $\overline{^4He}$ mass peaks. Thus including the TOF allows the sample of $\overline{^4He}$ to be increased from 4 to 18 events.

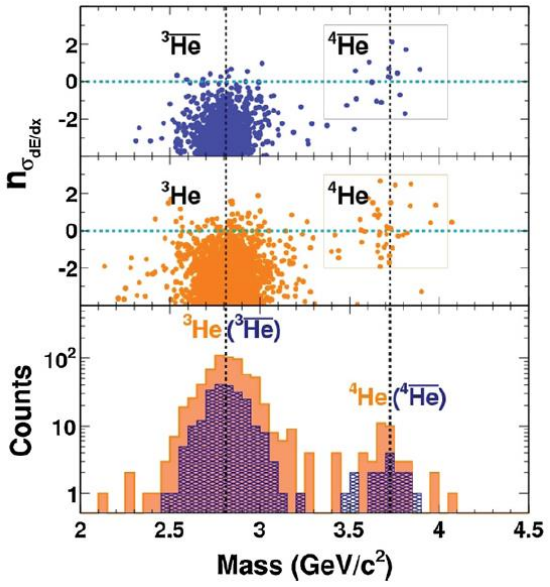

Figure 5. The top two panels show the dE/dx in units of multiples of $\sigma_{\mathrm{dE/dx}}$, $n_{\sigma_{\mathrm{dE/dx}}}$, of negatively charged particles (first panel) and positively charged particles (second panel) as a function of mass

measured by the TOF system. The bottom panel shows a projection of entries in the upper two panels onto the mass axis for particles in the window of $-2 < \sigma_{dE/dx} < 3$.

3.2. CBM experiment in GSI

The Compressed Baryonic Matter spectrometer (CBM) [34] is a heavy-ion experiment located at the Facility for Anti-proton and Ion Research (FAIR) in Darmstadt, Germany. The goal of the CBM research program is to explore the QCD (Quantum Chromo-Dynamics) phase diagram in the region of high baryon densities using high-energy nucleus-nucleus collisions. This includes the study of the equation-of-state of nuclear matter at neutron star core densities and the search for phase transitions, chiral symmetry restoration and exotic forms of (strange) QCD matter. The CBM detector is designed to measure the collective behavior of hadrons, together with rare diagnostic probes such as multi-strange hyperons, charmed particles and vector mesons decaying into lepton pairs with unprecedented precision and statistics. In order to produce high statistics data even for the particles with the lowest production cross sections, the CBM experiment is designed to run at reaction rates of up to 10 MHz. Such unprecedented rates requires very fast and radiation hard detectors, a novel data readout and analysis concept including free streaming front-end electronics, and a high performance computing cluster for online event selection.

3.2.1. The CBM-ToF system

The CBM ToF wall [35, 36] is composed of MRPC detector. A time resolution of the system below 80 ps and an overall efficiency above 95% are necessary to provide charged hadron identification (protons, kaons and pions) up to a particle momentum of about 4 GeV/c in the angular range between 2.5° and 25°. In order to accumulate enough statistics of rare probes the CBM detector has to run at ion beam intensities up to 10^9/s. Thus, the most challenging requirement for the detector is the capability to cope with rates between 0.5 kHz/cm² and 20 kHz/cm² depending on their location. These high rate requirements are no longer achievable with MRPCs built in the standard technique with float glass resistive plates. The rate capability [37, 38] is mainly limited by the current that can flow through the high resistivity electrodes and can be improved working on a number of interconnected parameters. Reducing the electrode thickness and the average charge delivered in the gas gap are possible ways to improve the rate capability, but the effects are not remarkable. A natural way is to search for low resistivity materials for the electrode plates so that the operating current can be increased without reducing the voltage applied to the gas.

A kind of low resistive glass [39, 40] was developed in Tsinghua University, Beijing, China. The parameters of the low resistive glass is shown in Table 2. It's bulk resistivity is about $10^{10}\ \Omega \cdot cm$. In order to meet the requirement of CBM-ToF, around 1000 square meters of low resistive glass are produced, shown in Figure 6. Under the restriction of the glass composition and processing technology, the dimensions of one piece of low resistivity glass is limited to 32 cm x 30 cm. Large area detectors can be achieved by the mosaic MRPC [41], which is built by directly combining pieces of the resistive glass together in each layer. Similar MRPC prototypes based on such low resistive glass were produced and tested by the beam in ELBE, Dresden-Rossendorf, Germany, to examine their performance under high rate. As shown in Figure 7, the efficiency is still higher than 90% and the time resolution is about 80 ps at 70 kHz/cm² rate [39].

Table 2. The parameters of the low resistive glass performance.

Performance	Parameters
Bulk resistivity	$\sim 10^{10}\ \Omega \cdot cm$
Standard thickness	0.7 mm, 1.1 mm
Thickness uniformity	20 μm
Surface roughness	< 10 nm
Maximal dimension	32 cm x 30 cm
Dielectric constant	7.5 ~ 9.5

DC measurement	Ohmic behavior stable up to 1 C/cm²

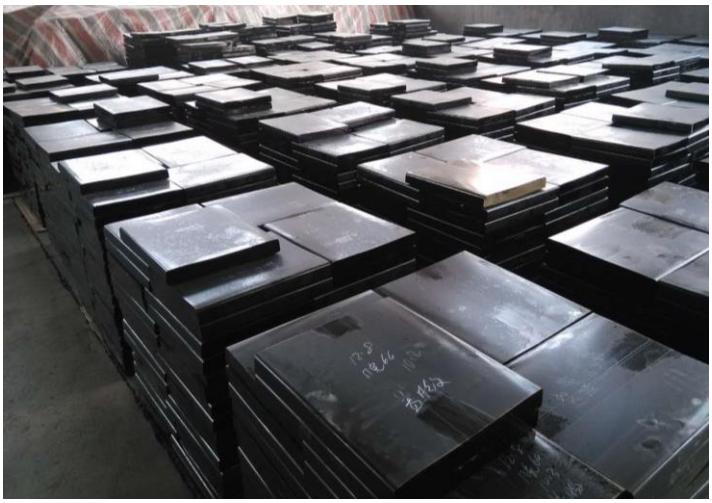

Figure 6. Low resistive glass strips for mass production.

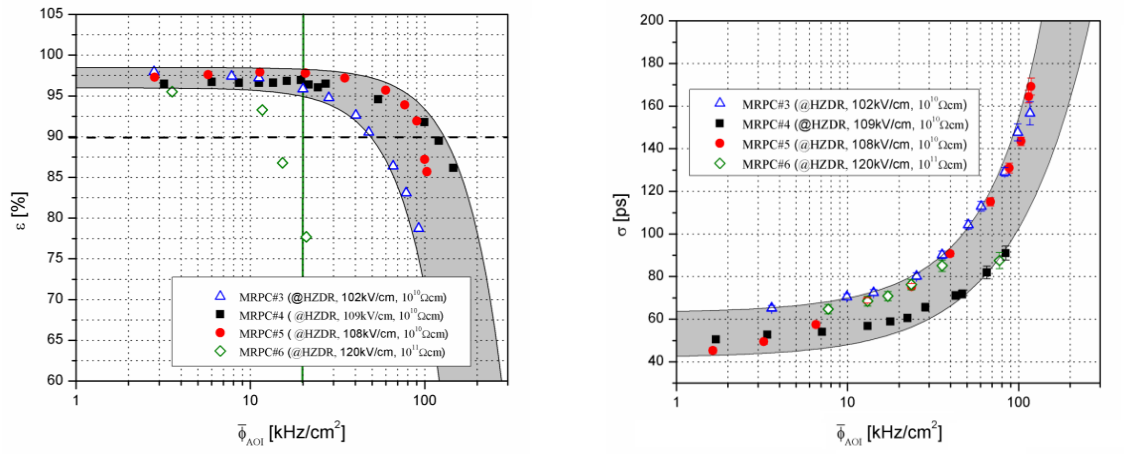

(a) **(b)**

Figure 7. Measured efficiencies **(a)** and time resolutions **(b)** for high rate MRPCs as a function of the average particle flux determined with reference scintillators.

The high performance electronics for the whole CBM ToF wall is based on the PADI [42] and the GET4-ASIC chips [43] developed by the CBM-ToF group. The PADI board has 32 channels and the threshold can be set via slow control. It can be directly connected to the MRPC readout electrodes inside the gas box, which suppresses the electromagnetic induced noise from outside and matches the impedance from electrodes to the pre-amplifier itself.

3.2.2. High-rate MRPC

Aiming at the region where the particle flux ranges from 1 and 5 kHz/cm², the double-ended readout strip MRPC prototype [9] developed at Tsinghua University have been developed. It is built by the low resistive glass plates described above. This MRPC has 2 x 4 gaps with 250 um gap size and 32 readout strips, each of 1 x 27 cm². The results of SPS beam time in 2015 for prototypes were presented in Ref. [9]. The 13A GeV Ar beam is applied and the rate has increased to 1 kHz/cm². The detector performance in different runs are depicted in Figure 8. The efficiency and time resolution curves correspond well to the changes of high voltage and PADI threshold. The efficiency is stable at the working point and maintains above 97% for all the run time. The system time resolution tends to improve with time at the beginning and reaches a value of about 85 ps. The

first batch production of 73 MRPC counters [44] have been produced and installed into STAR-eToF and the ToF system at mini-CBM.

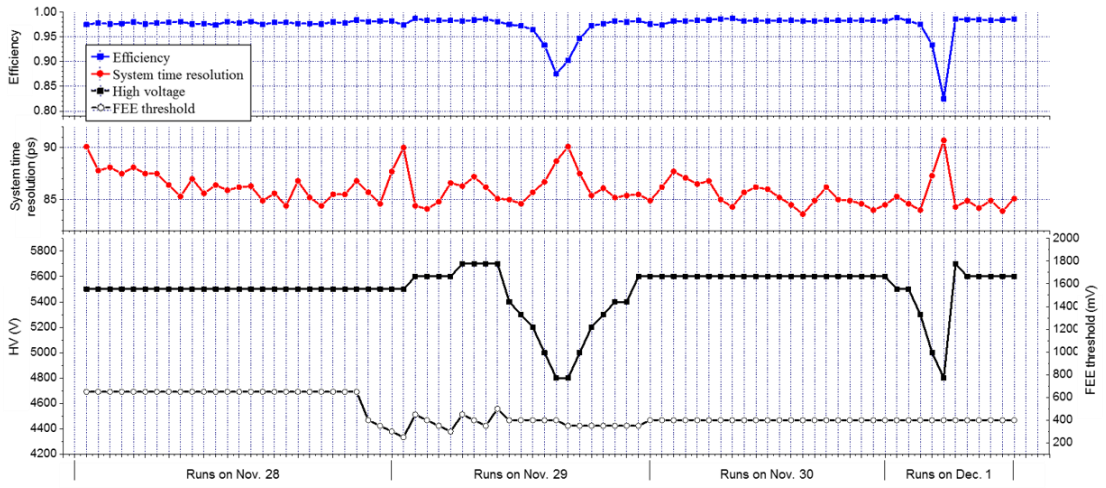

Figure 8. The detector performance in different runs for the MRPC3a prototypes.

3.2.3. FAIR Phase 0 programs

In order to create an environment where all aspects of the developed detector systems can be elaborated under real battle conditions the FAIR Phase 0 program [45] was carried out. The idea is to install and operate existing FAIR related detector equipment in running experiments all over the world. CBM TOF subsystem participates in two FAIR Phase 0 programs, which will be discussed in the following.

mCBM (mini-CBM) is full-system test-setup for CBM located at the SIS18 facility of GSI/FAIR. The primary goal is to test and optimize the performance of the detector subsystems including the operation of the detector prototypes in a high-rate environment, the free-streaming data acquisition system, the online track and event reconstruction as well as event selection algorithms, the offline data analysis and the detector control system. Therefore, it will significantly reduce the commissioning time for CBM at SIS100. mTOF performance during mCBM beam time in 2019 can be found in [46].

The endcap Time-of-Flight (eTOF) project comprises the installation, commissioning and operation of 10% of the full CBM TOF modules positioned at the STAR apparatus during the Beam Energy Scan II (BESII) campaign and the participation in the data analysis. The eTOF upgrade [47] covers the rapidity range from -1.1 to -1.6 for the collider collision mode, while for the fix target collision mode the PID extension is between 1.6 and 2.1, which is absolutely essential in order to cover the mid-rapidity range.

eTOF consist of 36 modules grouped in 12 sectors which are arranged in 3 layers in a wheel spokes structure around the beam axis. 12 modules are equipped with counters from type MRPC2 while 24 modules have counters from type MRPC3. Each module houses 3 MRPCs which leads to a total of 108 counter and 6912 read out channels. The full hardware installation was completed in Nov. 2018. After a commissioning phase of about 10 weeks the first data taking started in Feb. 2019 by recording about 580 M Au+Au events at $\sqrt{s_{NN}} = 11.5\ GeV$ with an eTOF efficiency of 85%. The readout system for eTOF is using the free-streaming architecture and hardware and software

components. It comprises 216 PADI (preamplifier and discriminator) and 216 GET4 (TDC) boards (for 108 counters).

After offline calibration of the TPC and eTOF the matching efficiency of MRPC hits in respect to the extrapolated TPC tracks can be deduced as function of the particle momentum. Figure 9(a) is obtained by evaluating the system time resolution with relativistic pions. Both counter type show results in the order of 85 ps. The good time resolution is reflected in the 1/β versus the particle momenta plot shown in Figure 9(b) which is generated with $\sqrt{s_{NN}} = 7.7\ GeV$ fix target data. The narrow particle bands allow for a kaon to pion separation of up to a momentum of 2.5 GeV/c which demonstrates the excellent PID capability of eTOF.

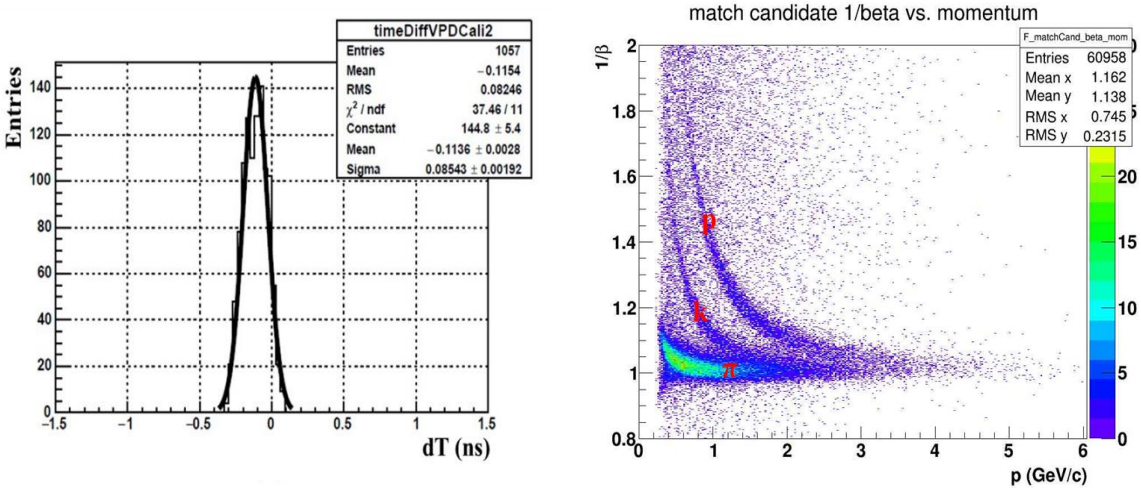

(a) **(b)**

Figure 9. (a) System time resolution obtained with relativistic pions. **(b)** 1/β as a function of particle momentum.

3.3. Developments for future ToF systems

3.3.1. High rate and ultrahigh time resolution MRPC

Although the science of the electromagnetic force between the atomic nucleus and the electrons is well understood but we still know little about nucleon's structure and the quarks and gluons that make up the protons and neutrons of nuclei. The future experiments with higher luminosity and beam energy, such as the 12 GeV program of JLab [48, 49] and the Electron-Ion Collider (EIC) [50] at Brookhaven Lab, will provide a powerful tool and simultaneously impose strict requirements on the detector devices. For example, the requirements for the TOF wall of the SoLID experiment [51, 52] at JLab include a rate capability up to 10 kHz/cm² with a time resolution of 20 ps, which allows the ToF to do kaon identification over a momentum range of 1 GeV/c to 7 GeV/c. For the future EIC detector at BNL, a 10 ps ToF [53] would provide π/K separation up to 7 GeV at the typical distances of 4 m available on the hadron-going side.

Thus, a number of R&D projects currently have been putting effort into investigating high performance detectors. M.C.S. Williams et al. [54] from the LHC-ALICE group developed a 24-gap MRPC with a gap width of 160 um. It was constructed as four stacks, each with six gas gaps. The resistive plates were made of soda-lime glass sheets of 400 mm thickness. Using the NINO front end electronics and the oscilloscope-based DAQ system, time resolution of 27 ps for cosmic ray test and 21 ps for beam test has been obtained.

Two Chinese groups (Tsinghua University and USTC) [51] have committed to perform R&D and construct the required detector for SoLID-ToF. Same as the CBM-ToF, low resistive silicate

glass will be employed as the resistive plates to achieve a high rate capability. To improve the time resolution, a detailed Monte Carlo simulation of the MRPC detector has been built and carried out [55, 56]. In the simulation framework, the energy deposition produced by particles passing through the detector is simulated based on the Photo Absorption Ionization (PAI) model [57], which is proved to be effective for very thin absorbers. The ionized electrons drifting to the anode will start the avalanche multiplication following Townsend effect [58] under the applied electric field as soon as they are created and induce a current signal on the read out electrodes according to Ramo theory [59]. The frontend electronics (FEE) response and noise can be included to study the detector performance under different experimental setup. By analyzing the simulation data and full signal information, performance of detectors with different structures at various working conditions can be easily studied.

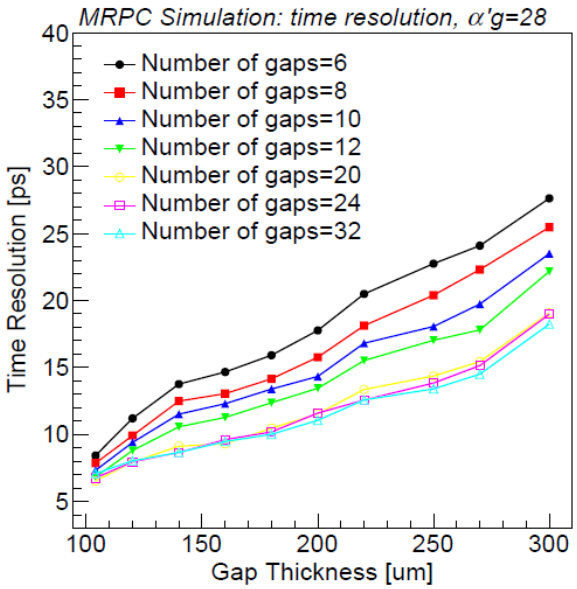

Figure 10. The time resolution of MRPCs with different thickness and numbers of the gas gaps [60].

Figure 10 [60] shows the intrinsic time resolution of MRPCs with different detector geometry. In this simulation, the effective Townsend coefficient times the gap thickness are fixed at $\alpha' g = 28$ to control the avalanche size and avoid streamers. It is obvious that thinner and more gaps have a much better time resolution. Besides, to reach the goal of 20 ps time resolution, the possible choices for future MRPCs are mainly the designs with thickness below 160 cm and at least 20 gas gaps, which ensures the intrinsic resolution of the detector below 10ps. In general, gaps in this kind of MRPCs are divided into several stacks and the voltage is added separately on each stack. Figure 11 shows the time resolution as a function of the number of stacks in a detector. We can see that when the detector is divided into more stacks, the time resolution becomes larger. It is because that more stacks mean a much thicker chamber and a longer distance between the very first and last gaps, which will lead to a larger variance of the starting time for each avalanche.

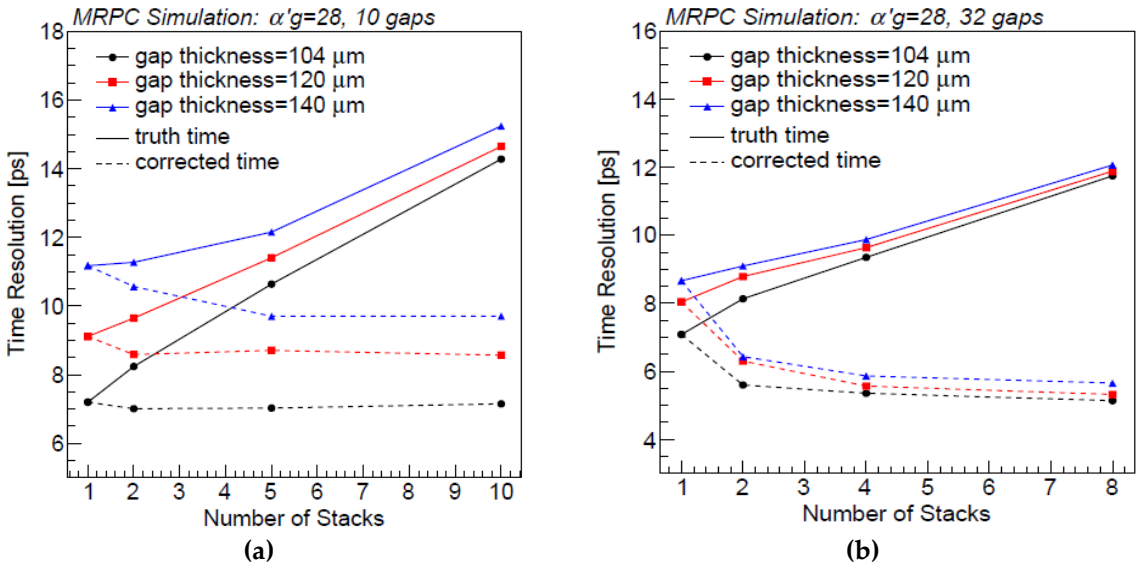

Figure 11. The time resolution of MRPCs with different number of stacks in a detector. The total number of gaps are fixed to be 10 in **(a)** and 32 in **(b)**. [60]

Based on the Monte Carlo simulation and the above study, a 32-gap MRPC detector [61] has been developed. As shown in Figure 12(a), it is divided into 4 stacks, each stack with 8 gaps. The thickness of the gas gaps is only 104 μm. The PCB sheets were divided into 6 readout strips on a 7 mm pitch with 3 mm separating each strip from its neighbour. Five PCBs were used in this design: a central anode pcb, two intermediate cathode PCBs and two outer anode PCBs. The anode and cathode signals generated on these boards are connected by pins to the central PCB and thus a differential signal is collected. During the preliminary cosmic ray test, the high-performance Analog Frontend Electronics (AFE) [62] from USTC and the Lecroy oscilloscope were used. The time distribution is shownd in Figure 13(b) and the time resolution can reach 20 ps at the electric field of 150 kV/cm. Now they are working on the new MRPCs with low resistive glass to reach both high time resolution and high rate.

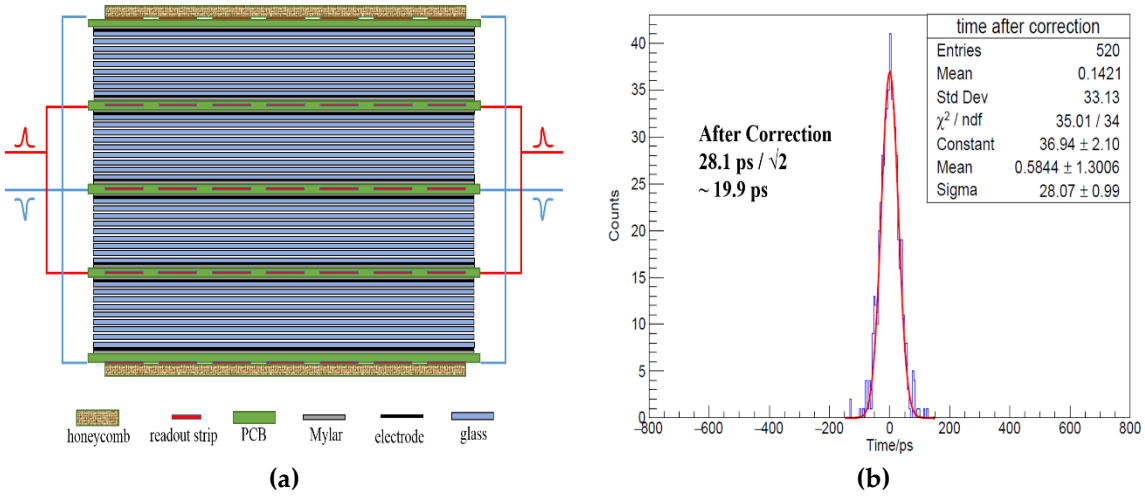

Figure 12. (a) Schematic drawing of the cross-section of the 32-gap MRPC. **(b)** Time resolution results after the slewing correction.

3.3.2. New time reconstruction algorithm

In recent times, artificial neural networks (ANNs) as one type of model for machine learning (ML), has become popular and helpful model for classification, clustering, pattern recognition and

prediction in many fields including the high energy physics analysis [63-66]. For present MRPCs, the signal is usually read out using the Time-Over-Threshold (ToT) method as mentioned before. The main drawback is that the uncertainty of each TDC channel is typically around 20 ps, which is large enough to overwhelm the intrinsic MRPC resolution. Besides, the threshold crossing time is related to the pulse amplitude, so the time-slewing effect should be carefully corrected. F. Wang [67] proposed an end-to-end solution to reconstruct the MRPC time with neural network (NN) algorithms. The Monte Carlo simulation described before provided labeled training datasets to train the network model, while the experiment datasets are used to test. Two kinds of networks FC (fully-connected) and LSTM (the Long Short Term Memory network) are detailed studied. And they both give a more accurate and precise time resolution results compared to the ToT method.

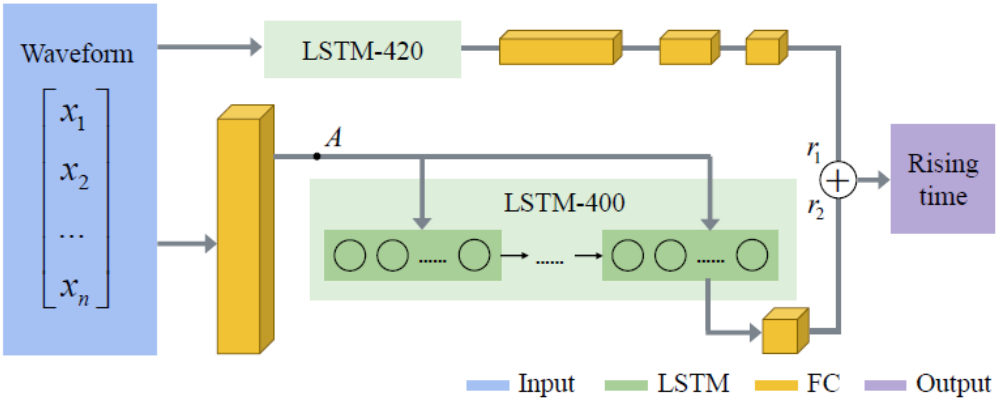

Figure 13. The structure of the ComLSTM network.

F. Wang [68] also proposed a ComLSTM (Combined LSTM) neural network (see Figure 13), which combines the advantages of both the LSTM and FC. The detailed description of the ComLSTM structure can be found in [68]. For the 32-gap MRPC same as [61], timing performances with both the ComLSTM neural network and the traditional threshold based method are shown below. The best time resolution with the ComLSTM can reach $23.82/\sqrt{2} = 16.84\,ps$, which is better than that of the ToT method. Although the neural networks have shown a better performance, much efforts need to be put into implementing and validating them in the high-energy physics and particle experiments.

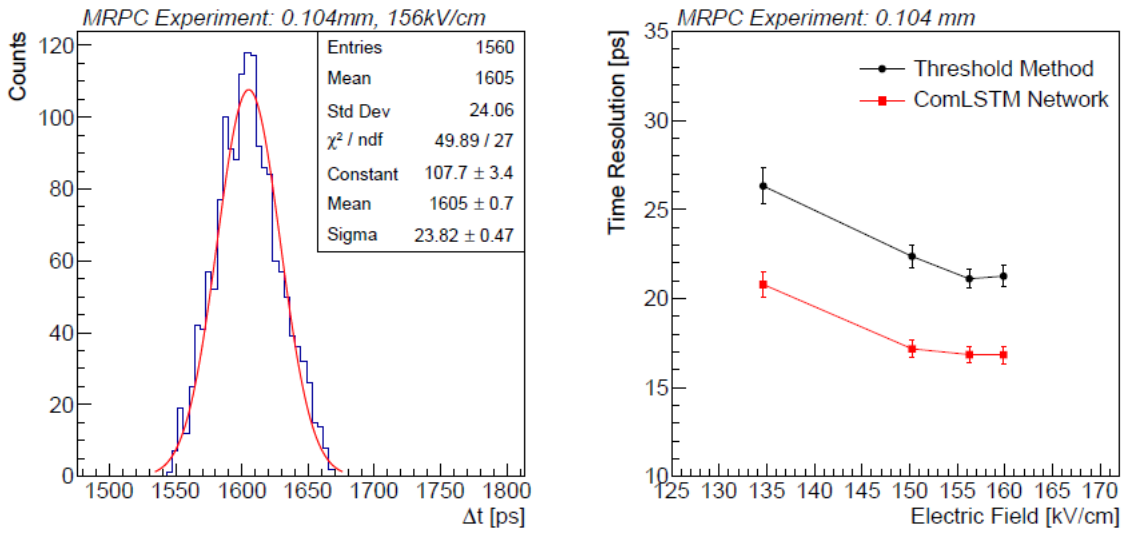

Figure 14. The time resolution of the 32-gap MRPC [76]. **(a)** Time distribution at $E = 156$ kV/cm for the ComLSTM neural network. **(b)** Time resolution as a function of the electric field. The black markers and curves shows the results given by the threshold method, while the red markers and curves given by the ComLSTM.

3.4. Brief summary

The main properties of the MRPC detectors used in large experiments are summarized in Table 3. The efficiency of all these MRPCs is very close to 100%, which is quite good. MRPCs with a gap thickness of around 0.25 mm can reach a time resolution of 60 ps, while much thinner gaps and higher working field can lead to a time resolution better than 20 ps. The rate capability of MRPCs made of float glass sheet is typically below 1 kHz/cm^2. MRPCs based on the low resistive glass ($\rho \sim 10^{10}\ \Omega \cdot$ cm), which can reach a rate up to 70 kHz/cm^2, are considered by CBM and future experiments.

Table 3. Parameters and features of different MRPC detectors.

	ALICE	STAR	HADES	CBM	Future (SoLID)
Gap Thickness (mm)	0.25	0.22	0.3	0.25	0.1~0.16
Gas Gaps	2x5	1x6	1x4	2x4	4x8
Working Gas ($C_2H_2F_4/C_4H_{10}/SF_6$)	90/5/5	95/5/0	98.5/1/0.5	90/5/5	90/5/5
Working Field (kV/cm)	96	107	107	110	~150
Glass Type	Float	Float	Float	Low res.	Low res.
Detection Efficiency	99.9%	95%	95%	95%	95%
Time Resolution (ps)	60	60	70	60	20
Counting Rate (Hz/cm^2)	50	10	700	25k	10k

The main solutions for the readout electronics are based on the fast and low-power amplifier/discriminator and the TDCs, shown in Table 4. Their overall time jitters are usually around 20 ps. The time over threshold (ToT) method is used to get the arrival time of the signals and the time-amplitude effect should be corrected. For the future experiments such as SoLID and EIC, to achieve ultra-high time resolution, a very thin-gap MRPC detector and readout electronics of a fast low-noise preamplifier module and a waveform digitization module are proposed. Thanks to the full signal sampling techniques, neural networks can be used to reconstruct the detector time.

Table 4. Summary of the electronics and timing methods for MRPC detectors.

	Electronics	**Time Jitter/ps**	**Time Reconstruction Algorithm**
ALICE/STAR	NINO Amplifier HPTDC	~20 ~25	Time Over Threshold (ToT)
CBM	PADI GET4	~10 ~25	Time Over Threshold (ToT)
Future (SoLID)	Fast AFE Waveform Digitizer(SCA)	< 5 < 5	Neural Networks

4. Conclusions and Outlook

In summary, MRPC detector is currently a standard technology for time of flight system. This paper has reviewed its famous applications on ToF system in several experiments. The performances including the time resolution and particle identification have been described in detail. With the increase of accelerator energy and luminosity, the requirement for ToF system becomes harsher. The paper has discussed some recent advances and perspectives with regard to the future development of the next generation MRPC.

However, there are still some new requirements and unclear problems, which should be explored further in terms of the following aspects.

(1) Currently not ecologically compatible gases are used, a big research effort have been addressed to ecologically compatible gas mixtures.

(2) High rate and high space-time resolution MRPCs with integration and reliability would have a great potential for development and future applications.

Author Contributions: Y. W. and Y. Y. conceived the idea; Y. Y. wrote and edited the paper; Y. W. revised the paper. All authors have read and agreed to the published version of the manuscript.

Acknowledgments: The work is supported by National Natural Science Foundation of China under Grant No. U1832118, 11927901, 11420101004, 11461141011, 11275108, 11735009, and U1832118. This work is also supported by the Ministry of Science and Technology under Grant No. 2018YFE0205203, 2015CB856905, 2016 YFA0400100.

Conflicts of Interest: The authors declare no conflict of interest.

References

1. Lippmann, C. Particle identification. Nucl. Instrum. Methods A 2012, 666, 148-172.
2. Akimov, V.A.; Akindinov, V.A.; Boyarinov, S.V.; Voloshin, K.G.; Vorob'ev, L.S.; Grishuk, Yu.G.; Zagreev, B.V.; Kats, M.M.; Kiselev, S.M.; Kuleshov, S.V.; et al. A Parallel-Plate Chamber as a Detector for Time-of-Flight Measurements. Instruments and Experimental Techniques 2002, 45, 493-500.
3. Akimov, V.A.; Akindinov, V.A.; Boyarinov, S.V.; Voloshin, K.G.; Vorob'ev, L.S.; Grishuk, Yu.G.; Zagreev, B.V.; Kats, M.M.; Kiselev, S.M.; Kuleshov, S.V.; et al. Studying the Characteristics and Optimizing the Parameters of a Parallel-Plate Chamber Used As a Detector for Time-of-Flight Measurements. Instruments and Experimental Techniques 2004, 47, 589-597.
4. Rizzo, A.; Narici, L.; Messi, R.; Cipollone, P.; De Donato, C.; Di Fino, L.; Iannillia, M.; La Tessa, C.; Manea, C.; Masciantonio, G.; et al. A compact Time-Of-Flight detector for space applications: The LIDAL system. Nucl. Instrum. Methods A 2018, 898, 98-104.
5. Akindinov, A.; Alici, A.; Antonioli, P.; Arcelli, S.; Baek, Y.W.; Basile, M.; Cara Romeo, G.; Cifarelli, L.; Cindolo, F.; De Caro, A.; et al. Final test of the MRPC production for the ALICE TOF detector. Nucl. Instrum. Methods A 2009, 602 709-712.
6. Akindinov, A.; Alici, A.; Antonioli, P.; Arcelli, S.; Basile, M.; Bellini, F.; Caffarri, D.; Cara Romeo, G.; Cifarelli, L.; Cindolo, F.; et al. The MRPC-based ALICE Time-Of-Flight detector: Commissioning and first performance. Nucl. Instrum. Methods A 2012, 661 S98-S101.
7. Wang, X.Z.; Sun, Y.J.; Li, C.; Heng, Y.K.; Wu, Z.; Cao, P.; Dai, H.L.; Ji, X.L.; Gong, W.X.; Liu, Z.; et al. The upgrade system of BESIII ETOF with MRPC technology. Journal of Instrumentation 2016, 11, pp. C08009.
8. Deppner, I.; Herrmann, N.; Akindinov, A.; Bartos, D.; Balaceanu, A.; Belogurov, S.; Cao, P.; Caragheorgheopol, G.; Chen, H.; Cheng, J.; et al. The CBM Time-of-Flight wall — a conceptual design, Journal of Instrumentation 2014, 9, pp. C10014.
9. Wang, Y.; Lyu, P.; Huang, X.; Han, D.; Xie, B.; Li, Y.; Herrmann, N.; Deppner, I.; Simon, C.; Loizeau, P.-A.; et al. Development and test o f a real-size MRPC for CBM-TOF. Journal of Instrumentation 2016, 11, pp. C08007.
10. Bonner, B.; Eppley, G.; Lamas-Valverde, J.; Llope, W.J.; Nussbaum, T.; Platner, E.; Roberts, J.; CerronZeballos, E.; Hatzifotiadou, D.; Kim, N.Y.; et al. A multigap resistive plate chamber prototype for time-of-flight for the STAR experiment at RHIC. Nucl. Instrum. Methods A 2002, 478, 176-179.
11. Bonner, B.; Chen, H.; Eppley, G.; Geurts, F.; Lamas-Valverde, J.; Li, Ch.; Llope, W.J.; Nussbaum, T.; Platner, E.; Roberts, J. A single Time-of-Flight tray based on multigap resistive plate chambers for the STAR experiment at RHIC. Nucl. Instrum. Methods A 2003, 508, 181-184.

12. Wang, Y.; Wang, J.B.; Cheng, J.P.; Li, Y.J.; Yue, Q.; Chen, H.S.; Li, J. Production and quality control of STAR-TOF MRPC. Nucl. Instrum. Methods A 2010, 613, 200-206.
13. Park S. Production of RPC gaps for the PHENIX upgrade. Nucl. Instrum. Methods A 2012, 661, S82-S85.
14. Santonico, R.; Cardarelli, R. Development of resistive plate counters. Nucl. Instrum. Methods A 1981, 187, 377-380.
15. Cerron Zeballos, E.; Crotty, I.; Hatzifotiadou, D.; Lamas Valverde, J.; Neupane, S.; Williams, M. C. S.; Zichichi, A. A new type of resistive plate chamber: the multigap RPC. Nucl. Instrum. Methods A 1996, 374, 132-136.
16. Riegler, W.; Lippmann, C.; Veenhof, R. Detector physics and simulation of Resistive Plate Chambers. Nucl. Instrum. Methods A 2003, 500, 144-162.
17. Fonte, P. Survey of physical modelling in Resistive Plate Chambers. Journal of Instrumentation 2013, 8, pp. P11001.
18. Lippmann, C.; Riegler, W. Space charge effects in Resistive Plate Chambers. Nucl. Instrum. Methods A 2004, 517, 54-76.
19. Lippmann, C.; Riegler, W. Detailed RPC avalanche simulations. Nucl. Instrum. Methods A 2004, 533, 11-15.
20. Abbrescia, M; Colaleo, A; Iaselli, G; Loddo, F; Maggi, M; Marangelli, B; Natali, S; Nuzzo, S; Pugliese, G; Ranieri, A; et al. Progresses in the simulation of resistive plate chambers in avalanche mode. Nucl. Phys. B Proc. Suppl. 1999, 78, 459-464.
21. Harrison, M.; Ludlam, T.; Ozaki, S. RHIC project overview. Nucl. Instrum. Methods A 2003, 499, 235-244.
22. STAR Collaboration. The STAR Experiment at the Relativistic Heavy Ion Collider. Nuclear Physics A 1994, 566, 277c-286c.
23. The STAR TOF Collaboration. Proposal for a Large Area Time of Flight System for STAR. Available online: https://www.star.bnl.gov/public/tof/publications/TOF_20040524.pdf (accessed on 1 July 2020).
24. Anghinolfi, F.; Jarron, P.; Krummenacher, F.; Usenko, E.; Williams, M.C.S. NINO: an ultrafast low-power front-end amplifier discriminator for the time-of-flight detector in the ALICE experiment. IEEE Transactions on Nuclear Science 2005, 51, 1974-1978.
25. Anghinolfi, F.; Jarron, P.; Martemyanov, A.N.; Usenko, E.; Wenninger, H.; Williams, M.C.S.; Zichichi, A. NINO: an ultra-fast and low-power front-end amplifier/discriminator ASIC designed for the multigap resistive plate chamber. Nucl. Instrum. Meth. A 2004, 533, 183-187.
26. Christiansen J. High performance time to digital converter manual. Available online: https://tdc.web.cern.ch/TDC/hptdc/docs/hptdc_manual_ver2.2.pdf (accessed on 1 July 2020).
27. Mota, M.; Christiansen, J.; Debieux, S.; Ryjov, V.; Moreira, P.; Marchioro, A. A flexible multichannel high-resolution time-to-digital converter ASIC. 2000 IEEE Nuclear Science Symposium Conference Record 2002, 2, 9/155 -9/159.
28. Schambach, J.; Hoffmann, G.; Kajimoto, K.; Bridges, L.; Eppley, G.; Liu, J.; Llope, B.; Nussbaum, T.; Mesa, C. Star Time of Flight Readout Electronics, Daq, and Cosmic Ray Test Stand. International Journal of Modern Physics E 2007, 16, 2496-2502.
29. Llope, W.J.; STAR Collaboration. Multigap RPCs in the STAR experiment at RHIC. Nucl. Instrum. Methods A 2012, 661, S110-S113.
30. STAR Collaboration. Pion, kaon, proton and anti-proton transverse momentum distributions from p+p and d+Au collisions at s= 200 GeV. Physics Letters B 2005, 616, 8-16.
31. Shao, M.; Barannikova, O.; Dong, X.; Fisyak, Yu.; Ruan, L.; Sorensen, P.; Xu, Z. Extensive Particle Identification with TPC and TOF at the STAR Experiment. Nucl. Instrum. Methods A 2006, 558, 419-429.
32. Adams, J.; Aggarwal, M.M.; Ahammed, Z.; Amonett, J.; Anderson, B.D.; Arkhipkin, D.; Averichev, G.S.; Badyal, S.K.; Bai, Y.; Balewski, J.; et al. Open Charm Yields in d+Au Collisions at √(sNN)=200 GeV. Phys. Rev. Lett. 2005, 94, id. 062301.
33. Star Collaboration; Agakishiev, H.; Aggarwal, M.M.; Ahammed, Z.; Alakhverdyants, A.V.; Alekseev, I.; Alford, J.; Anderson, B.D.; Anson, C.D.; Arkhipkin, D.; et al. Observation of the antimatter helium-4 nucleus. Nature 2011, 473, 353-356.
34. Friese, V. The CBM experiment at GSI/FAIR. Nuclear Physics A 2006, 774, 377-386.
35. Herrmann, N. Technical Design Report for the CBM Time-of-Flight System (TOF). Available online: http://repository.gsi.de/record/109024 (accessed on 6 July 2020).

36. Deppner, I.; Herrmann, N. The CBM Time-of-Flight system. Journal of Instrumentation 2019, 14, pp. C09020.
37. Santonico, R. Development of a new generation of Resistive Plate Chambers for high radiation environment. ECFA high luminosity LHC experiments workshop, 21-23 Oct 2014.
38. Carboni, G.; Collazuol, G.; De Capua, S.; Domenici, D.; Ganis, G.; Messi, R.; Passaleva, G.; Santovetti, E.; Veltri, M. A model for RPC detectors operated at high rate, Nucl. Instrum. Methods A 2003, 498, 135-142.
39. Wang, J.; Wang, Y.; Gonzalez-Diaz, D.; Chen, H.; Fan, X.; Li, Y.; Cheng, J.; Kaspar, M.; Kotte, R.; et al. Development of high-rate MRPCs for high resolution time-of-flight systems. Nucl. Instrum. Meth. A 2013, 713, 40-51.
40. Wang, Y.; Zhang, Q.; Lyu, P.; Han, D.; Guo, B.; Li, Y. Development and Production of High Rate MRPC for CBM TOF. JPS Conf. Proc. 2019, 26, 024006.
41. Yu, Y.; Han, D.; Wang, Y.; Guo, B.; Lyu, P.; Chen, X.; Shen, C.; Wang, F.; Li, Y.; Cimmino, A.; et al. R&D of a real-size Mosaic MRPC within the framework of the CMS muon upgrade. Journal of Instrumentation 2019, 14, pp. C10042.
42. Ciobanu, M.; Herrmann, N.; Hildenbrand, K.D.; Kis, M.; Schuttauf, A.; Flemming, H.; Deppe, H.; Lochner, S.; Fruhauf, J.; Deppner, I.; Loizeau, P.A.; Trager, M. PADI, an Ultrafast Preamplifier - Discriminator ASIC for Time-of-Flight Measurements. IEEE Trans. Nucl. Sci. 2014, 61, 1015-1023.
43. Deppe, H.; Flemming, H. The GSI event-driven TDC with 4 channels GET4. IEEE Nucl. Sci. Symp. Conf. Rec. 2009, 295-298.
44. Lyu, P.; Han, D.; Wang, Y.; Zhang, Q.; Guo, B.; Wang, F.; Yu, Y.; Chen, X.; Li, Y.; Herrmann, N.; et al. Study on cosmic test and QC method of high-rate MRPC for CBM-TOF. Journal of Instrumentation 2019, 14, pp. C09032.
45. Deppner, I.; Herrmann, N. The FAIR Phase 0 program of the CBM TOF. arXiv: 2006.08510.
46. Zhang, Q.; Deppner, I.; Herrmann, N.; Wang, Y. mTOF performance during mCBM beam time at GSI. arXiv:2006.00388.
47. The STAR Collaboration and the CBM Collaboration eTOF Group. Physics Program for the STAR/CBM eTOF Upgrade. arXiv:1609.05102v1.
48. Dudek, J.; Ent, R.; Essig, R.; Kumar, K.S.; Meyer, C.; McKeown, R.D.; Meziani, Z.E.; Miller, G.A.; Pennington, M.; Richards, D.; et al. Physics opportunities with the 12 gev upgrade at jefferson lab. The European Physical Journal A 2012, 48, id. 187.
49. Cardman, L.S.; JLab 12 GeV project team. The JLAB 12 GEV energy upgrade of CEBAF for QCD and hadronic physics. IEEE Particle Accelerator Conference 2007, Conf.Proc.C 070625, 58-62.
50. Accardi, A.; Albacete, J.L.; Anselmino, M.; Armesto, N.; Aschenauer, E.C.; Bacchetta, A.; Boer, D.; Brooks, W.K.; Burton, T.; et al. Electron-Ion Collider: The next QCD frontier. Eur. Phys. J. A 2016, 52, id. 268, 100 pp.
51. The SoLID Collaboration. SoLID (Solenoidal Large Intensity Device) Updated Preliminary Conceptual Design Report. Available online: https://hallaweb.jlab.org/12GeV/SoLID/download/doc/solid_precdr_2017.pdf (accessed on 6 July 2020).
52. The SOLID collaboration; Chen, J.P.; et al. A White Paper on SoLID (Solenoidal Large Intensity Device). arXiv:1409.7741.
53. Electron-Ion Collider Detector Requirements and R&D Handbook, February, 2020. Available online: http://eicug.org/web/sites/default/files/EIC_HANDBOOK_v1.1.pdf (accessed on 16 June 2020).
54. An, S.; Jo, Y.K.; Kim, J.S.; Kim, M.M.; Hatzifotiadou, D.; Williams, M.C.S.; Zichichi, A.; Zuyeuski, R.A. 20 ps timing device—A Multigap Resistive Plate Chamber with 24 gas gaps. Nucl. Instrum. Meth. A 2008, 594, 39-43.
55. Wang, F.; Han, D.; Wang, Y.; Yu, Y.; Zhang, Q.; Guo, B.; Li, Y. A standalone simulation framework of the MRPC detector read out in waveforms. Journal of Instrumentation 2018, 13, pp. P09007.
56. Yu, Y.; Han, D.; Wang, Y.; Wang, F.; Chen, X.; Lyu, P.; Guo, B.; Shen, C.; Zhang, Q.; Li, Y. The simulation and application of three-dimensional electrostatic weighting field in MRPC detector. Journal of Instrumentation 2019, 14, pp. P07020.
57. Apostolakis, J.; Giani, S.; Urban, L.; Maire, M.; Bagulya, A.V.; Grichine, V.M. An implementation of ionisation energy loss in very thin absorbers for the GEANT4 simulation package, Nucl. Instrum. Meth. A 2000, 453, 597-605.

58. Townsend, J.S. The conductivity produced in gases by the motion of negatively-charged ions. Nature 1900, 62, 340-341.
59. Ramo, S. Currents induced by electron motion. Proc. IRE 1939, 27, 584-585.
60. Wang, F.; Han, D.; Wang, Y.; Lyu, P.; Li, Y. A detail study on the intrinsic time resolution of the future MRPC detector. Nucl. Instrum. Meth. A 2020, 950, id. 162932.
61. Yu, Y.; Han, D.; Wang, Y.; Guo, B.; Wang, F.; Chen, X.; Lyu, P.; Shen, C.; Zhang, Q.; Li, Y. Study of high time resolution MRPC with the waveform digitizer system, Journal of Instrumentation 2020, 15, pp. C01049.
62. Liu, J.; Zhao, L.; Yan, L.; Li, Z.; Liu, S.; An, Q. Design of a prototype readout electronics with a few picosecond time resolution for MRPC detectors, Nucl. Instrum. Meth. A 2019, 925, 53-59.
63. Baldi, P.; Sadowski, P.; Whiteson, D. Searching for exotic particles in high-energy physics with deep learning. Nat. Commun. 2014, 5, id. 4308.
64. de Oliveira, L.; Kagan, M.; Mackey, L.; Nachman, B.; Schwartzman, A. Jet-images — deep learning edition. J. High Energ. Phys. 2016, 2016, id.69, 32 pp.
65. Dan, G.; Kyle, C.; Daniel, W. Deep Learning and Its Application to LHC Physics. Annual Review of Nuclear and Particle Science 2018, 68, 161-181.
66. Amrouche, S.; Braun, N.; Calafiura, P.; Farrell, S.; Gemmler, J.; Germain, C.; Gligorov, V.V.; Golling, T.; Gray, H. Track reconstruction at LHC as a collaborative data challenge use case with RAMP. Eur. Phys. J. Web Conf. 2017, 150, id. 00015.
67. Wang, F.; Han, D.; Wang, Y.; Yu, Y.; Guo, B.; Li, Y. A neural network based algorithm for MRPC time reconstruction. Journal of Instrumentation 2019, 14, pp. C07006.
68. Wang, F.; Han, D.; Wang, Y. Improving the time resolution of the MRPC detector using deep-learning algorithms. arXiv:2005.03903.